

THE LLM SURGEON

Tycho F.A. van der Ouderaa^{1*}, Markus Nagel², Mart van Baalen²,

Yuki M. Asano³, Tijmen Blankevoort²

¹Imperial College London, ²Qualcomm AI Research[†], ³QUVA Lab, University of Amsterdam

ABSTRACT

State-of-the-art language models are becoming increasingly large in an effort to achieve the highest performance on large corpora of available textual data. However, the sheer size of the Transformer architectures makes it difficult to deploy models within computational, environmental or device-specific constraints. We explore data-driven compression of existing pretrained models as an alternative to training smaller models from scratch. To do so, we scale Kronecker-factored curvature approximations of the target loss landscape to large language models. In doing so, we can compute both the dynamic allocation of structures that can be removed as well as updates of remaining weights that account for the removal. We provide a general framework for unstructured, semi-structured and structured pruning and improve upon weight updates to capture more correlations between weights, while remaining computationally efficient. Experimentally, our method can prune rows and columns from a range of OPT models and LlamaV2-7B by 20%-30%, with a negligible loss in performance, and achieve state-of-the-art results in unstructured and semi-structured pruning of large language models.

1 INTRODUCTION

Recent advancements in language modeling (Vaswani et al., 2017) allow fitting large language models (LLMs) with millions or even billions of parameters (such as OPT (Zhang et al., 2022) and Llama 2 (Touvron et al., 2023)) on big text corpora achieving high performance. Unfortunately, the size of these LLMs often makes it hard to deploy them within practical constraints. Cloud-based deployment can get very expensive for larger models, and efficient devices such as phones are frequently limited in the memory size to host a model.

A body of literature extending back to the late 1980s, e.g., Optimal Brain Damage (OBD, LeCun et al. (1989)) and Optimal Brain Surgeon (OBS, Hassibi & Stork (1992)), phrases pruning as a constraint optimization problem to reduce a model’s footprint and runtime requirements. The Hessian required for this approach grows with the square of the number of parameters, and can only be computed in practice for unrealistically small networks. To overcome this issue, Eigendamage (Wang et al., 2019) introduces a Kronecker factorization of a blockwise-diagonal approximation of the Hessian. Recent works, like Optimal Brain Compression (Frantar & Alistarh, 2022) and SparseGPT (Frantar & Alistarh, 2023), demonstrate practical post-training pruning of LLMs, but only consider a loss curvature of a pruned layer’s squared output reconstruction error, ignoring gradients that relate local removal costs to the target loss. As a result, their approximation to the target loss landscape

*Work done while doing an internship at Qualcomm AI Research

[†]Qualcomm AI Research is an initiative of Qualcomm Technologies, Inc.

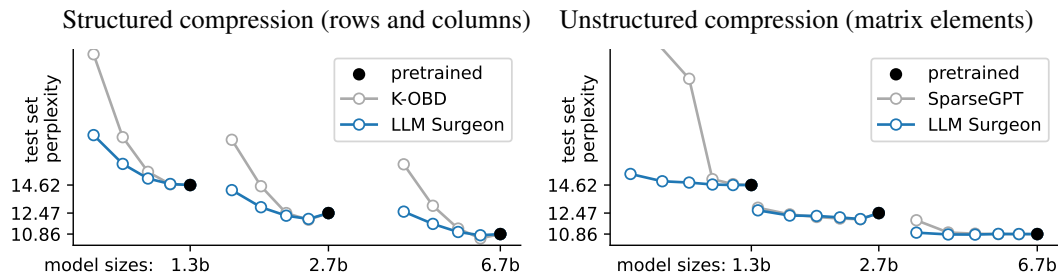


Figure 1: LLM Surgeon allows interpolation of model size between existing pretrained models.

is inaccurate, leading to a significant performance degradation for pruned LLMs. Further, these methods do not readily extend to structured pruning.

This work introduces LLM Surgeon, a general framework for unstructured, semi-structured and structured pruning of LLMs. To the best of our knowledge, this is the first method to successfully perform structured pruning for LLMs. This is achieved by scaling up the block-diagonal Kronecker-factorized approximations to the empirical Fisher from Eigendamage to LLMs. We further expand upon the work by deriving OBS-like weight pruning costs and updates for structured pruning of multiple rows and columns, and provide a general framework that also incorporates semi-structured and unstructured pruning. Instead of treating individual weight updates independently, we strive to consider as many correlations between weights as practically possible and derive joint weight updates for pruning multiple weights (or multiple sets of structured weights) at once. Unlike prior work in LLM pruning, LLM Surgeon prunes in multiple shots, updating weights and curvature estimates between shots. We use global thresholding for unstructured, semi-structured and structured, i.e., instead of pruning layers by a fixed amount, more sensitive layers are pruned less than those that are more robust. Lastly, we propose to mitigate possible first-order gradients not being zero by using optional low-rank first-order updates between shots. A key advantage of LLM Surgeon is that it allows trading off additional compute during compression for better accuracy by increasing the number of correlations and/or shots. Our method gives the first practically usable results for structured pruning of LLMs – they can be pruned by up to 30% with minor performance degradation. Furthermore, we achieve state-of-the-art results in unstructured and semi-structured LLM pruning.

2 BACKGROUND AND RELATED WORK

Neural network pruning aims to remove parameters from a model while minimizing negative impact on final performance. More formally, we denote the P model parameters as vector $\boldsymbol{\theta}^* = \text{vec}(\mathbf{W}_1^*, \mathbf{W}_2^*, \dots, \mathbf{W}_L^*) \in \mathbb{R}^P$, by flattening the L weight matrices of attention and fully-connected blocks, with already fitted $\boldsymbol{\theta}^* \approx \arg \min_{\boldsymbol{\theta}} \mathcal{L}(\boldsymbol{\theta})$ to data \mathcal{D} to minimise a negative likelihood loss $\mathcal{L}(\boldsymbol{\theta}) = -\log p(\boldsymbol{\theta} | \mathcal{D})$. To compress the model, we are looking for a pruned vector $\hat{\boldsymbol{\theta}}$:

$$\hat{\boldsymbol{\theta}} = \arg \min_{\boldsymbol{\theta}} \mathcal{L}(\boldsymbol{\theta}) \text{ s.t. pruning constraints based on } \boldsymbol{\theta}^* \quad (1)$$

where chosen constraints determine the structure of compressed weights $\hat{\boldsymbol{\theta}}$. In **unstructured pruning**, a fraction of total weight elements is set to zero. In **semi-structured pruning** of M:N we have that M weights of every N consecutive weights are zero (Zhou et al., 2021; Hubara et al., 2021). And in **structured pruning** (Louizos et al., 2017), entire rows and columns are set to zero. Structured pruning leads to the most immediate gains in memory and compute, as it directly reduces the dimensions of matrices that need to be represented explicitly, but is typically regarded as a more difficult compression task. Maintaining high performance is often easier in the other schemes, but requires specialised arithmetic exploiting the sparsity structure to benefit at deployment. We consider all pruning types above, with a focus on structured pruning for LLMs.

Typically, eq. (1) can not be solved directly, as the space of possible pruning configurations exceeds what can be evaluated in practice. To illustrate, a search over all possible unstructured pruning masks of a 125 million parameter LLM would require $2^P = 2^{125m} \approx 10^{37628749}$ evaluations. The idea, therefore, is to find $\hat{\boldsymbol{\theta}}$ using a surrogate of the loss landscape q that is easier to work with:

$$\mathcal{L}(\boldsymbol{\theta}) = -\log p(\mathcal{D} | \boldsymbol{\theta}) \approx -\log q(\boldsymbol{\theta}) \quad (2)$$

If one chooses a particular Gaussian form for our surrogate q , then solutions for unstructured, semi-structured, and structured pruning constraints can be derived in closed-form (appendix A).

2.1 TAYLOR EXPANSION

How do we obtain a good surrogate of the loss q ? One of the easiest approaches is to locally expand the log loss through a second-order Taylor expansion around the pretrained weights $\boldsymbol{\theta}^*$, yielding:

$$-\log q(\boldsymbol{\theta}) \approx -\log p(\mathcal{D} | \boldsymbol{\theta}^*) - (\boldsymbol{\theta} - \boldsymbol{\theta}^*)^T \nabla \mathcal{L}(\boldsymbol{\theta}^*) - \frac{1}{2} (\boldsymbol{\theta} - \boldsymbol{\theta}^*)^T \mathbf{H}_{\boldsymbol{\theta}^*} (\boldsymbol{\theta} - \boldsymbol{\theta}^*) \quad (3)$$

where $[\nabla \mathcal{L}(\boldsymbol{\theta}^*)]_i = \frac{\partial}{\partial \boldsymbol{\theta}_i} \mathcal{L}(\boldsymbol{\theta}^*)$ denotes the Jacobian and $[\mathbf{H}_{\boldsymbol{\theta}}]_{ij} = \frac{\partial^2}{\partial \boldsymbol{\theta}_i \partial \boldsymbol{\theta}_j} \mathcal{L}(\boldsymbol{\theta}^*)$ denotes the Hessian. The first-order term vanishes $[\nabla \mathcal{L}(\boldsymbol{\theta}^*)]_i = \mathbf{0}$ at the optimum. Note that in practice the first order

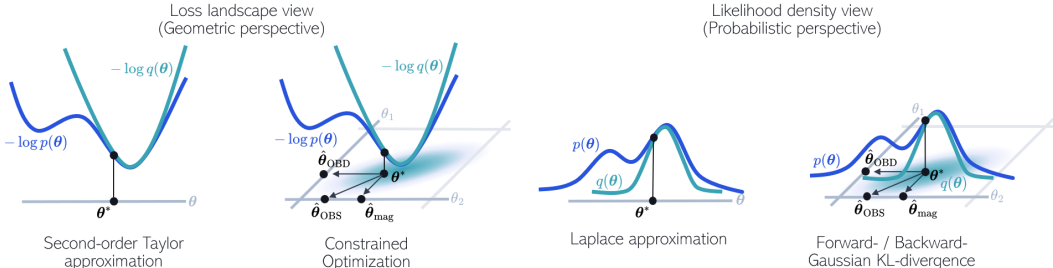


Figure 2: Pruning as equality constrained optimization of quadratic approximation of the loss landscape (left), or equivalently, maximising the likelihood under a Laplace approximation (right).

term may not vanish. While we follow this assumption initially, we consider interleaved first-order corrections to mitigate the issue in section 3.6. The quadratic expansion of eq. (3) forms the basis of the optimal brain damage (LeCun et al., 1989) and optimal brain surgeon (Hassibi & Stork, 1992) pruning methods. Note that from a probabilistic perspective, a quadratic approximation of the log likelihood implies a Gaussian approximation of the likelihood, as also observed by (Wang et al., 2019) and illustrated in fig. 2. This is well-known (Bishop & Nasrabadi, 2006), (MacKay, 2003) as the Laplace approximation $q(\theta) = \mathcal{N}(\theta | \theta^* + \nabla \mathcal{L}(\theta^*), \mathbf{H}_{\theta^*}^{-1})$, with pretrained weights are the mean and the local inverse Hessian is the covariance matrix capturing *correlations between weights*.

2.2 BLOCK FISHER INFORMATION MATRIX

For a network trained with negative log-likelihood loss, the Hessian is identical to the Fisher matrix:

$$\mathbf{H}_{\theta} = \mathbf{F}_{\theta} = \sum_{n=1}^N \mathbb{E}_{y \sim p_{\theta}(y|x_n)} [\nabla_{\theta} \log p_{\theta}(y|x_n) \nabla_{\theta} \log p_{\theta}(y|x_n)^T] \quad (4)$$

which has the benefit of always being positive semi-definite, with the inverse thus forming a proper covariance matrix for q , and can be approximated with Monte Carlo samples of $p_{\theta}(y|x_n)$. For most LLMs, this would be treating the softmax output of the network as categorical distribution $p_{\theta}(y|x_n)$, and sampling from that. In practice, we use the ‘empirical Fisher’ replacing the expectation over y with target data y_n (Kunstner et al., 2019). The full (empirical) Fisher $\mathbf{F}_{\theta} \in \mathbb{R}^{P \times P}$ scales quadratically in the number of parameters P . To overcome this, the Fisher is often written in terms of layer-wise blocks $\mathbf{F}_{lk} = \sum_{n=1}^N \mathbb{E} [\text{vec}(\nabla_{\mathbf{W}_l} \log p_{\theta}(y|x_n)) \text{vec}(\nabla_{\mathbf{W}_k} \log p_{\theta}(y|x_n))^T]$, and approximated by only treating layers independently (Martens & Grosse, 2015; Botev et al., 2017):

$$\mathbf{F}_{\theta} = \text{diag}(\mathbf{F}_{11}, \mathbf{F}_{22}, \dots, \mathbf{F}_{LL}), \quad \mathbf{F}_l = \sum_{n=1}^N \mathbb{E} \left[\underbrace{(\mathbf{g}_{l,n} \mathbf{g}_{l,n}^T) \otimes (\mathbf{a}_{l,n} \mathbf{a}_{l,n}^T)}_{RC \times RC} \right] \quad (5)$$

where \otimes denotes the Kronecker product and $\text{vec}(\cdot)$ the matrix vectorisation operation. Because we disregard cross-layer interactions we write \mathbf{F}_l instead of \mathbf{F}_{ll} for Fisher blocks associated with the weight matrix $\mathbf{W}_l \in \mathbb{R}^{R \times C}$ producing outputs $\mathbf{y}_{l,n} = \mathbf{W}_l \mathbf{a}_{l,n} \in \mathbb{R}^R$ from inputs $\mathbf{a}_{l,n} \in \mathbb{R}^C$, for each layer l and datapoint n . Consequently, we can compute Fisher blocks from input activations $\mathbf{a}_{l,n} \in \mathbb{R}^C$ of forward-passed data x_n and output gradients $\mathbf{g}_{l,n} = \nabla_{\mathbf{y}_{l,n}} \mathcal{L} \in \mathbb{R}^R$ from backpropagation.

2.3 PRUNING AS CONSTRAINED OPTIMIZATION

Optimal brain surgery relies on removing and adapting weights such that the loss is least negatively affected, thus it behoves us to write the problem as a constrained optimization problem. From the Gaussian approximation discussed in section 2.1 obtained by quadratically expanding the log likelihood loss $-\log p \approx \frac{1}{2} \theta^T \mathbf{F} \theta$, the optimal update $\Delta \theta = \hat{\theta} - \theta$ (and thus also $\hat{\theta} = \theta + \Delta \theta$) becomes the following equality constrained quadratic optimization problem (Hassibi & Stork, 1992):

$$\begin{aligned} \arg \min_{\Delta \theta} \quad & \frac{1}{2} \Delta \theta^T \mathbf{F} \Delta \theta \\ \text{s.t.} \quad & \mathbf{e}_k^T \Delta \theta + \mathbf{e}_k^T \theta = 0, \forall k \in \mathcal{K} \end{aligned} \quad (6)$$

where \mathbf{F} is positive semi-definite and \mathcal{K} is the set of K indices that are pruned (i.e., set to zero).

Algorithm 1 LLM Surgeon (*structured*)

Input: initial weights θ^0 , target size α , and data \mathcal{D}

For shot t in $[1, 2, \dots, T]$

- Compute:** approximate curvature \mathbf{G}, \mathbf{A} from data \mathcal{D} ▷ section 3.1
- Compute:** costs per row/column $\mathcal{L}_r, \mathcal{L}_c$ from \mathbf{G}, \mathbf{A} ▷ section 3.2
- Compute:** threshold τ using \mathcal{L}_r and \mathcal{L}_c given target size α_t ▷ section 3.3
- Select:** rows and columns to remove $\mathbf{E}_R, \mathbf{E}_C$ based on τ ▷ section 3.3
- Compute:** weight update $\Delta\theta^{t-1}$ based on $\mathbf{E}_R, \mathbf{E}_C$ and \mathbf{G}, \mathbf{A} ▷ section 3.4
- Update:** remaining weights $\theta^t \leftarrow \theta^{t-1} + \Delta\theta^{t-1}$ ▷ section 3.5
- Optionally:** $\theta^t \leftarrow$ low-rank update(θ^t) ▷ section 3.6

Output: compressed weights $\hat{\theta} = \theta^T$

General solution We denote $\mathbf{E}_K = [\mathbf{e}_1 \ \mathbf{e}_2 \ \dots \ \mathbf{e}_K]^T \in [0, 1]^{K \times P}$ as a matrix of which the row vectors are canonical basis vectors $\mathbf{e}_k \in \mathbb{R}^P$ that select the elements to be pruned. One of the most standard approaches to solve eq. (6) is using Langrange multipliers, which results in a general closed-form solution for the expected increase in loss \mathcal{L} and optimal weight update $\Delta\theta$:

$$\mathcal{L} = \frac{1}{2}(\mathbf{E}_K \theta^*)^T (\mathbf{E}_K \mathbf{F}^{-1} \mathbf{E}_K^T)^{-1} \mathbf{E}_K \theta \quad (7)$$

$$\Delta\theta = -\mathbf{F}^{-1} \mathbf{E}_K^T (\mathbf{E}_K \mathbf{F}^{-1} \mathbf{E}_K^T)^{-1} \mathbf{E}_K \theta \quad (8)$$

which we use to derive unstructured, semi-structured, structured for modern Fisher approximations (see appendices A.2 to A.4). The same general form of eqs. (7) and (8) appears in prior LLM pruning work Kurtic et al. (2022), but only for much simpler layer-wise pruning and no structured pruning.

3 LLM SURGEON

This section describes the components of our method, **LLM Surgeon**, summarised in algorithm 1.

3.1 ESTIMATING LOSS LANDSCAPE CURVATURE

Accurate pruning relies on approximating the local curvature accurately while overcoming the memory cost associated with storing the true curvature. Specifically, even with the block-wise approximation of eq. (5), $\mathbf{F} \in \mathbb{R}^{RC \times RC}$ requires summing N large $RC \times RC$ matrices, too large to practically fit in memory. Instead, we adapt the KFAC approximation (Martens & Grosse, 2015) that assumes independence of activations and derivatives, approximating an expectation of Kronecker products as a Kronecker product of two expectations $\mathbb{E}[\mathbf{g}_{l,n} \mathbf{g}_{l,n}^T \otimes \mathbf{a}_{l,n} \mathbf{a}_{l,n}^T] \approx \mathbb{E}[\mathbf{g}_{l,n} \mathbf{g}_{l,n}^T] \otimes \mathbb{E}[\mathbf{a}_{l,n} \mathbf{a}_{l,n}^T]$, allowing layer-wise Fisher blocks to be approximated as $\mathbf{F}_l \approx \tilde{\mathbf{F}}_l$, where

$$\tilde{\mathbf{F}}_l = \mathbf{G}_l \otimes \mathbf{A}_l \quad , \text{with } \mathbf{G}_l = \frac{1}{\sqrt{N}} \sum_{n=1}^N \mathbf{g}_{l,n} \mathbf{g}_{l,n}^T \text{ and } \mathbf{A}_l = \frac{1}{\sqrt{N}} \sum_{n=1}^N \mathbf{a}_{l,n} \mathbf{a}_{l,n}^T \quad (9)$$

constructed from activations $\mathbf{a}_{l,n} \in \mathbb{R}^C$ from forward passes and gradients $\mathbf{g}_{l,n} \in \mathbb{R}^R$ from backward passes. The approximation was originally proposed for optimization, but has recently gained popularity for other problems that require curvature approximations (Immer et al., 2022), including structured pruning in Wang et al. (2019).

An additional advantage of approximating Fisher blocks as Kronecker products is that the inverse becomes particularly easy to compute $\tilde{\mathbf{F}}^{-1} = \mathbf{G}^{-1} \otimes \mathbf{A}^{-1}$, thus only requires inverting the factors. This fact allows us to never explicitly construct large $RC \times RC$ matrices in memory that make up \mathbf{F} and $\tilde{\mathbf{F}}^{-1}$, but rather directly work with the much smaller matrices \mathbf{G} and \mathbf{A} .

3.2 COMPUTING COSTS IN FINAL LOSS

The number of possible combinations in which weights can be removed grows (supra-)exponentially in parameter count, making it infeasible to estimate a separate cost \mathcal{L} for each such removal. A common strategy, therefore, is to treat weights independently when computing removal costs \mathcal{L} . We also follow this strategy, but note that this does not necessarily imply that we have to make such same strong independence assumption for the weight updates $\Delta\theta$ after selecting weights to be removed.

Unlike most prior work, we present correlated weight updates by taking into account off-diagonal elements of the Fisher approximation in section 3.4.

For semi-structured and unstructured we use independent costs for individual weight elements $k \in [1, RC]$, and for structured use independent costs for all rows $r \in [1, R]$ and columns $c \in [1, C]$. We find that we can derive the appropriate costs from the general cost formula eq. (7) by letting $\mathbf{E} = \mathbf{e}_k \in \mathbb{R}^{RC}$ where the single one-hot element at index k of canonical basis vector \mathbf{e}_k selects the weight to remove. For structured pruning, we similarly select rows r and columns c , by setting $\mathbf{E} = \mathbf{e}_r^T \otimes \mathbf{I} \in \mathbb{R}^{C \times RC}$ or $\mathbf{E} = \mathbf{I} \otimes \mathbf{e}_c \in \mathbb{R}^{R \times RC}$ with $\mathbf{e}_r \in \mathbb{R}^R$, $\mathbf{e}_c \in \mathbb{R}^C$. Plugging into eq. (7), we find:

$$\mathcal{L}_k = \frac{1}{2} \frac{(\theta_k)^2}{[\mathbf{G}^{-1} \otimes \mathbf{A}^{-1}]_{kk}}, \quad \mathcal{L}_r = \frac{1}{2} \frac{\theta_r^T \mathbf{A} \theta_r}{[\mathbf{G}^{-1}]_{rr}}, \quad \mathcal{L}_c = \frac{1}{2} \frac{\theta_c^T \mathbf{G} \theta_c}{[\mathbf{A}^{-1}]_{cc}} \quad (10)$$

Full derivations can be found in appendices A.2 and A.3. The costs for single elements \mathcal{L}_k are equivalent to those found in optimal brain surgeon (Hassibi & Stork, 1992) and \mathcal{L}_r and \mathcal{L}_c closely resemble structured brain surgeon of (Wang et al., 2019), but in our case derived for matrix rows and columns (see appendix A.3). Given curvature estimates, costs for either removing all weights or all rows and columns can be computed in parallel. In addition, we derive costs for the more general sum of Kronecker factor approximation $\tilde{\mathbf{F}} \approx \mathbf{G}_1 \otimes \mathbf{A}_1 + \mathbf{G}_2 \otimes \mathbf{A}_2$ in appendix I through an eigendecomposition.

3.3 DYNAMIC WEIGHT ALLOCATION WITH GLOBAL THRESHOLD

Unlike prior works that compress layer-by-layer (Frantar & Alistarh, 2023), we use a global threshold τ enabling a *dynamic allocation of sparsity levels across layers*, pruning most where it hurts the least. Our method can compress a model to a specifically chosen target size α , defined as the fraction of weights that should remain, i.e. stay non-zero after compression. In all structured, semi-structured, and unstructured pruning (fig. 3), we select as many

weights for removal so that the target size α is reached that inflict the least possible costs \mathcal{L} , as computed according to section 3.2. For unstructured pruning, this is as simple as sorting the costs for all weights \mathcal{L}_k in the network and setting a global threshold τ such that α fraction of weights fall within the threshold $\mathcal{L}_k \leq \tau$. For M:N semi-structured pruning, we sort the M costs of each N consecutive weights and select the M weights with lowest cost. In case of a multi shot schedule (see section 3.5) we also sum the M lowest costs in each block to find a cost per block, sort costs per block across the entire network, and similar to the unstructured case set a global threshold τ such that an α fraction of weights fall within threshold. Lastly for structured pruning, we perform a sorting appropriately weighted by the number of elements that make up a row or column and set the global threshold τ such that α fraction of all weights fall within the threshold. Then we remove all rows and columns that fall within the threshold $\mathcal{L}_r, \mathcal{L}_c \leq \tau$.

3.4 CORRELATED WEIGHT UPDATES

Like most other pruning methods, we prune multiple weights at once (Frantar & Alistarh, 2023; Wang et al., 2019). To arrive at pruning costs and weight updates for pruning multiple weights, it is common to compute costs and updates for individual weights (or sets of weights) independently and add them together to arrive at a joint pruning cost. In LLM Surgeon, we argue that it's better to consider weight updates jointly instead of independently. After selecting the set of weights for pruning, we can often afford to compute a single correlated weight update associated to the joint removal of multiple weights, instead of naively summing weight updates associated to individual removals. We derive such correlated weight updates below. Note that, for the expected cost computation, we do assume that the row, column or weight costs are independent, as the number of possible combinations of weights to prune grows too large to compute within reasonable time.

Fast unstructured / semi-structured correlated weight updates Mathematically, we represent pruned weights as $\mathbf{E}_K = [e_1 \ e_2 \ \dots \ e_{R'}]^T \in \mathbb{R}^{K \times RS}$, where $e_r \in \mathbb{R}^{R'}$ are one-hot canonical ba-

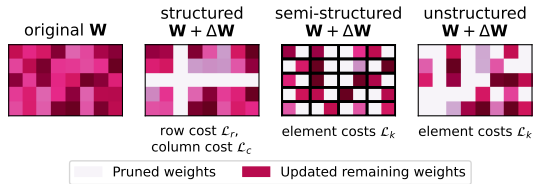


Figure 3: General framework for structured, semi-structured and unstructured compression.

sis vectors selecting the weights for removal. As each element k has a unique associated row r and column c index, we can consequently also use canonical basis vectors for these respective rows $\mathbf{E}_R \in \mathbb{R}^{K \times R}$ and columns $\mathbf{E}_C \in \mathbb{R}^{K \times C}$ (i.e., we have $[\mathbf{E}_R]_i \otimes [\mathbf{E}_C]_i = [\mathbf{E}_K]_i$ is satisfied for all i).

We derive unstructured weight updates in appendix A.2, by considering eigendecompositions $\mathbf{G} = \mathbf{K}_1 \mathbf{S}_1 \mathbf{K}_1^T$, $\mathbf{A} = \mathbf{K}_2 \mathbf{S}_2 \mathbf{K}_2$ of the Fisher approximation $\mathbf{F} \approx \mathbf{G} \otimes \mathbf{A}$, which from eq. (8) yields:

$$\Delta \mathbf{W} = \mathbf{G}^{-1} \left(\mathbf{K}_1 \left(\underbrace{\mathbf{K}_1^T \mathbf{W}^{-1} \mathbf{K}_2}_{K \times K} \otimes \mathbf{S} \right)^{-1} \mathbf{K}_2 \right) \mathbf{A}^{-1} \quad (11)$$

where \otimes is element-wise division, and for brevity use bar notation $\bar{\mathbf{K}}_1 = \mathbf{E}_K \mathbf{K}_1$, $\bar{\mathbf{K}}_2 = \mathbf{E}_K \mathbf{K}_2$, $\bar{\boldsymbol{\theta}} = \mathbf{E}_K \boldsymbol{\theta}$, and $\mathbf{S} = \text{diag}(\mathbf{S}_1) \text{diag}(\mathbf{S}_2)^T \in \mathbb{R}^{R \times C}$, and $\text{diag}(\cdot)$ vectorises matrix diagonals.

Programmatically, we always avoid explicitly representing large matrices $\tilde{\mathbf{F}}$ and $\tilde{\mathbf{F}}^{-1}$ in memory, but rather compute relevant quantities from their factors. Likewise, we never represent sparse matrices \mathbf{E}_K , \mathbf{E}_R or \mathbf{E}_C in memory, but instead work with a lists of indices of the one-hot elements directly. For example, we can cheaply construct $\bar{\mathbf{K}}_1 = \mathbf{E}_R \mathbf{K}_1 \in \mathbb{R}^{K \times R}$ and $\bar{\mathbf{K}}_2 = \mathbf{E}_C \mathbf{K}_2 \in \mathbb{R}^{K \times C}$, by copying row vectors, and the vector $\bar{\boldsymbol{\theta}} = \mathbf{E}_K \boldsymbol{\theta} = \mathbf{E}_R \mathbf{W} \mathbf{E}_C^T \in \mathbb{R}^K$ by indexing all pruned weights.

Maximum number of correlated weights The main computational bottleneck is the $K \times K$ matrix inverse in eq. (11). To control compression speed, we can split pruned weights into disjoint subsets $K = K_1 \cup K_2 \cup \dots$, such that each subset K_i does not exceed the set maximum number of correlated weights $K_i \leq m$, and sum associated independent updates. Using less correlation by setting a lower m allows trading compression quality for speed.

Fast structured correlated weight updates Unlike the general case which requires inverting a $K \times K$ matrix for K correlated weights, we find that weight updates with the Kronecker factored Fisher approximation $\tilde{\mathbf{F}} = \mathbf{G} \otimes \mathbf{A}$ only require inverting a $R' \times R'$ matrix when removing R' rows or a $C' \times C'$ matrix when removing C' columns. The updates are much cheaper than we would have expected based on the effective number of weights in those rows and columns, which would imply inverting $R'C \times R'C$ or $RC' \times RC'$ matrices. In practice, this leads to a significant speed-up for structured pruning and weight updates that take into account correlations between rows or columns. When removing R' rows, $r_1, r_2, \dots, r_{R'}$, or the C' columns $c_1, c_2, \dots, c_{C'}$, with $1 < R' < R$ and $1 < C' < C$, we denote one-hot vectors selecting all rows and columns to be removed respectively as $\mathbf{E}_{R'} = [e_1 \ e_2 \ \dots \ e_{R'}]^T \in \mathbb{R}^{R' \times R}$ and $\mathbf{E}_{C'} = [e_1 \ e_2 \ \dots \ e_{C'}]^T \in \mathbb{R}^{C' \times C}$. We find weight updates associated to removing the R' rows by setting $\mathbf{E}_K = \mathbf{E}_{R'} \otimes \mathbf{I}$ or $\mathbf{E}_K = \mathbf{I} \otimes \mathbf{E}_{C'}$:

$$\begin{aligned} \text{remove multiple } R' \text{ rows:} \quad \Delta \mathbf{W} &= -\bar{\mathbf{W}} (\mathbf{E}_{C'} \mathbf{A}^{-1} \mathbf{E}_{C'}^T)^{-1} (\mathbf{A}^{-1} \mathbf{E}_{C'}^T) \\ \text{remove multiple } C' \text{ columns:} \quad \Delta \mathbf{W} &= -\mathbf{G}^{-1} \mathbf{E}_{R'}^T (\mathbf{E}_{R'} \mathbf{G}^{-1} \mathbf{E}_{R'}^T)^{-1} \bar{\mathbf{W}} \end{aligned} \quad (12)$$

From here, it is clear that the special case of removing a single row r or column c under Kronecker approximation involves inverting a 1×1 matrix, and thus only requires scalar division:

$$\text{remove single row } r: \quad \Delta \boldsymbol{\theta} = -\frac{\mathbf{G}^{-1} \mathbf{e}_r \otimes \boldsymbol{\theta}_r}{[\mathbf{G}^{-1}]_{rr}} \quad , \text{ or single column } c: \quad \Delta \boldsymbol{\theta} = -\frac{\boldsymbol{\theta}_c \otimes \mathbf{A}^{-1} \mathbf{e}_c}{[\mathbf{A}^{-1}]_{cc}} \quad (13)$$

in accordance to independent structured updates in Wang et al. (2019), for convolutional filters. We have thus extended existing structured weight updates to rows and columns, and derived update rules that also consider correlation between structured groups (in our case the rows and columns).

3.5 MULTI SHOT PRUNING SCHEDULE

To improve the performance-to-sparsity ratio, we propose pruning in multiple shots. We theoretically justify this multi-shot approach by noting that the surrogate loss landscape q relies on a Taylor expansion (eq. (3)) that only holds locally and thus becomes unreliable for larger jumps $\Delta \boldsymbol{\theta}$ in parameter space. We mitigate this by pruning in multiple $T > 1$ shots, $t \in [1, 2, \dots, T]$, each resulting in a smaller weight update $\Delta \boldsymbol{\theta}$ after which the curvature of the loss surface can be re-estimated. When pruning to target size α , ie. removing $1 - \alpha$ of total weights, we choose a schedule α_t starting at $\alpha_0 = 1$ and ends with $\alpha_T = \alpha$, such that after T shots, exactly α fraction of the total weight remain. Empirically, we find that a linear schedule for α_t , as formulated in section 4, monotonically improves

Table 1: Structured compression of large language models on wikitext-2 data.

Method	Target size	Test performance (PPL)				
		OPT (125m)	OPT (1.3b)	OPT (2.7b)	OPT (6.7b)	LLama-v2 (7b)
Baseline	100%	27.65	14.62	12.47	10.86	5.12
Magnitude	90%	767.2	894.4	1229	3464	36746
$\mathbf{I} \otimes \mathbf{I}$	80%	4685	(1278)	2788	16747	347960
	70%	17970	(3098)	9255	17312	41373
L-OBD	90%	33.3	20.76	17.69	27.20	14259
diag($\mathbf{I} \otimes \mathbf{A}$)	80%	94.14	1392	3236	7570	15630
multi shot	70%	545.6	2147	7233	7628	21386
K-OBD	90%	27.97	14.68	11.96	10.53	5.48
diag($\mathbf{G} \otimes \mathbf{A}$)	80%	29.89	15.63	12.47	11.28	9.14
multi shot	70%	36.54	18.29	14.53	13.03	15.43
	60%	47.54	24.65	18.09	16.21	28.03
	50%	75.95	37.68	26.68	25.54	46.64
LLM Surgeon (ours)	90%	28.29	14.73	12.00	10.82	5.43
$\mathbf{G} \otimes \mathbf{A}$	80%	29.37	15.27	12.37	11.22	7.29
within row/col cor. Δ	70%	32.46	16.60	13.16	11.83	10.85
	60%	39.82	19.40	14.79	12.94	16.67
	50%	51.48	23.81	18.01	15.38	25.62
LLM Surgeon (ours)	90%	28.01	14.70	12.02	10.77	5.25
$\mathbf{G} \otimes \mathbf{A}$	80%	28.73	15.12	12.27	11.02	6.18
full cor. Δ	70%	31.82	16.24	12.92	11.64	7.83
	60%	38.47	18.45	14.23	12.58	10.39
	50%	49.78	22.95	17.15	14.90	15.38

pruning performance with more shots, and that higher sparsity levels typically require more shots (see appendix F.1). Multi-shot pruning allows one to spend (linearly in T) more computation to improve the final compression performance.

3.6 INTERLEAVED LOW-RANK FIRST-ORDER CORRECTIONS

We propose optional interleaved low-rank first-order corrections to further improve compression performance. So far, we assumed parameters are in a local optimum when finding a closed-form solution to the quadratic constraint problem. In practice, however, this assumption likely does not hold since (i) the neural network may not be optimised to the minimum, (ii) a different loss may be used for compression than used for training, or (iii) we prune in multiple shots (section 3.5) inevitably causing weights to diverge from the optimum. To mitigate this, we consider first-order corrections by interleaving pruning shots with low-rank adaptations of weights $\mathbf{W}_l + \mathbf{U}\mathbf{V}$ (LoRA, by (Hu et al., 2021)), commonly used in LLM finetuning. We always absorb updates after each shot, so that the next loss estimate q is closer to the optimum and underlying assumptions are likely to hold more closely. By absorbing LoRA updates between shots, the sum of low-rank updates can have a higher rank than individual updates. That is, we have $\text{rank}(\mathbf{U}^1\mathbf{V}^1 + \mathbf{U}^2\mathbf{V}^2 + \dots + \mathbf{U}^T\mathbf{V}^T) \geq \text{rank}(\mathbf{U}^t\mathbf{V}^t)$ for the updates $\mathbf{U}^t\mathbf{V}^t$ at any shot t , with equality only arising if updates lie exactly in the same subspace which is unlikely to ever occur in practice. This insight could also be used during regular LoRA finetuning and may therefore be useful outside the context of model compression to allow more expressive low-rank model adaptation, at negligible cost.

4 RESULTS

We compare compression performance of LLM Surgeon on language modeling tasks on OPT (Zhang et al., 2022) and Llama-v2 (Touvron et al., 2023) model families, using data from wikitext-2 dataset (appendix B.2). For compression, we use 128 sequences with a sequence length of 2048 tokens from the training data set and evaluate test perplexity (PPL) on the standard test split. In our experiments, we use a linear sparsity schedule $\alpha_t = 1 - t(\frac{1 - \alpha}{T})$ at each shot s before reaching the final sparsity α . We use 40 shots at $\alpha=0.5$ sparsity and report intermediate compression rates, effectively using $T=8$ shots for $\alpha=0.9$, $T=16$ for $\alpha=0.8$, $T=24$ for $\alpha=0.7$, and $T=32$ for $\alpha=0.6$. We compare against magnitude pruning, L-OBD, SparseGPT and K-OBD baselines. The K-OBD and LLM Surgeon use the multi shot procedure of section 3.5 using $T=40$ shots for structured pruning and $T=5$ shots for semistructured and unstructured pruning. Further details are found in appendix B.

4.1 STRUCTURED COMPRESSION

Structured compression of rows and columns enables direct savings in memory and compute through a straight reduction of matrix dimensions in the model. For LLM surgeon, we consider in section 3.4 weight updates with different levels of correlations: limited to correlations within rows and columns, and correlations both within and between rows and columns. We further compare against magnitude pruning, which only uses weight magnitudes, L-OBD, which only uses activations, and K-OBD, which also uses Kronecker-factored curvature but assumes full independence and thus only prunes without updating remaining weights. We report results in table 1, and observe that more correlations results in better performance, with the largest improvements for the Llama-v2 model family.

While a 50% structured compression is not better than a smaller model of similar size, LLM Surgeon allows us to reduce model size by up to 30% with minimal loss, without training a smaller model from scratch fig. 1. In our structured compression experiments our proposed LLM Surgeon method outperforms all baselines and achieves the best performance for each compression target size.

4.2 INTERLEAVED LOW-RANK UPDATES

Additionally, we assess compression performance in conjunction with the proposed first-order corrections using the interleaved low-rank adaptation described in section 3.6. We find that LoRA improves compression performance in the smallest 125m model, but not in larger models. We hypothesise that larger models are more prone to overfitting on the relatively few batches of wikitext-2 data used to compress the model. Nevertheless, we conclude that interleaved LoRA can be useful in cases, and recommend first using the proposed method without interleaved updates and, if enough data is available for compression, optionally using it if it improves performance.

4.3 SEMI-STRUCTURED COMPRESSION

For 2:4 semi-structured pruning, we compare LLM Surgeon with magnitude pruning, which only uses weight magnitudes, single-shot L-OBD, which only uses activations, and single-shot K-OBD, which also uses Kronecker-factored curvature but assumes full independence and thus only prunes without updating remaining weights as well as the recent state-of-the-art SparseGPT (Frantar & Alishtarh, 2023). We report test performance after 50 % (2:4) semi-structured compression on wikitext-2 data in table 3. We empirically find that considering more weight correlations results in improved final performance after compression. Our proposed LLM Surgeon is competitive with prior work outperforming all baselines in terms of test set perplexity (PPL).

Table 3: Semi-structured 2:4 compression for large language models on wikitext-2 data.

Method	$F \approx$	Target size	Test performance (PPL)			
			OPT (125m)	OPT (1.3b)	OPT (2.7b)	OPT (6.7b)
Baseline		100%	27.65	14.62	12.47	10.86
Magnitude	$I \otimes I$	50%	342.04	379.57	1106.01	187.29
L-OBD	$\text{diag}(I \otimes A)$	50%	87.26	44.92	41.40	27.36
K-OBD	$\text{diag}(G \otimes A)$	50%	68.74	27.22	20.23	15.55
SparseGPT	$I \otimes A$	50%	45.51	29.44	14.92	13.01
LLM Surgeon (ours)	$G \otimes A$	50%	44.64	25.10	14.64	12.10

4.4 UNSTRUCTURED COMPRESSION

For unstructured pruning, we repeat the same experiments as structured pruning case described in section 4.1. In table 4, we report final test performance in terms of perplexity (PPL) on wikitext-2 after compressing LLMs of different sizes of OPT and Llama-v2 family. Overall, we find that methods with more accurate approximations of the curvature landscape and that account for more correlations perform better. The proposed LLM Surgeon outperforms all baselines, reaching the highest test performance across target sizes.

Table 4: Unstructured compression of large language models on wikitext-2 data.

Method	Target size	Test performance (PPL)				
		OPT (125m)	OPT (1.3b)	OPT (2.7b)	OPT (6.7b)	Llama-v2 (7b)
Baseline	100%	27.65	14.62	12.47	10.86	5.12
Magnitude	90%	27.62	14.69	12.60	10.88	5.18
	80%	28.53	15.68	13.18	11.26	5.37
	70%	52.88	140.2	15.22	12.22	6.03
	60%	29.70	16.24	14.44	13.43	6.09
L-OBD	80%	32.18	21.92	23.35	39.85	116.2
	70%	49.08	204.7	274.8	810.4	6549
	60%	27.64	14.62	12.09	36.89	5.13
$\mathbf{G} \otimes \mathbf{A}$	80%	27.62	14.37	130220	39928	5.19
	70%	27.92	220.1	23097	19506	5.60
	60%	29.24	13783	10331	33896	9.20
	50%	34.43	7311	10495	91506	118.6
	40%	27.93	14.69	12.00	10.86	5.49
SparseGPT	80%	28.18	15.07	12.05	10.86	5.58
	70%	28.93	22.77	12.17	10.89	5.71
	60%	30.20	25.07	12.37	10.98	5.94
	50%	33.17	26.77	12.88	11.92	6.51
	40%	27.69	14.62	12.01	10.86	5.13
LLM Surgeon (ours)	80%	27.83	14.66	12.14	10.87	5.20
	70%	28.35	14.81	12.25	10.82	5.36
	60%	28.98	14.91	12.28	10.83	5.66
	50%	30.30	15.47	12.68	10.97	6.08
	40%	27.69	14.62	12.01	10.86	5.13

4.5 LEARNED SPARSITY STRUCTURE

The proposed method can dynamically allocate sparsity across layers through global thresholds described in section 3.3. In Fig. 4.5, we compare total allocated sparsity levels per layer depth and per layer type after compressing a pretrained OPT-125m model. We find that the LLM Surgeon prunes relatively more in the first layer and less in middle layers. Further, we observe that a larger portions of weights are removed in fully-connected compared to attention blocks, but deviations are less compared to other methods. Dynamic allocation allows for most pruning where it hurts least.

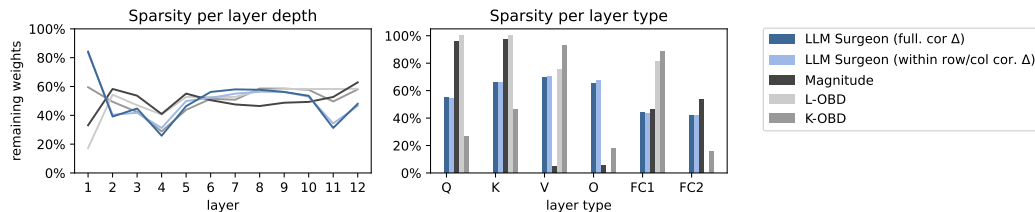


Figure 4: Sparsity levels obtained with structured pruning on OPT-125m by layer depth and type.

5 CONCLUSION

In this work, we have introduced the **LLM Surgeon** algorithm for unstructured, semi-structured and structured compression of neural networks. The work builds upon classic neural network compression approaches originating from the early 1990’s that aim to find optimal pruning by expanding the curvature of the loss landscape. The method utilises modern Fisher approximations to scale accurate pruning to the realm of large language models (LLMs) with billions of parameters, while remaining practical in both memory and compute. Unlike most prior work on data-based LLM compression, we not only use weight magnitude and activations from forward passes, but also use gradient information from backward passes to relate weight removal costs to the true final objective. We improve upon prior work through more accurate approximations to the loss landscape curvature and considering more weight correlations to update remaining weights. Increasing the number of correlations and using multiple shots allows us trading off additional compute for better accuracy. Lastly, LLM Surgeon gives the first practically usable results for structured pruning of LLMs and achieves state-of-the-art results in unstructured and semi-structured large language model pruning.

REFERENCES

Christopher M Bishop and Nasser M Nasrabadi. *Pattern recognition and machine learning*, volume 4. Springer, 2006.

Aleksandar Botev, Hippolyt Ritter, and David Barber. Practical gauss-newton optimisation for deep learning. In *International Conference on Machine Learning*, pp. 557–565. PMLR, 2017.

Elias Frantar and Dan Alistarh. Optimal brain compression: A framework for accurate post-training quantization and pruning. *Advances in Neural Information Processing Systems*, 35:4475–4488, 2022.

Elias Frantar and Dan Alistarh. Sparsegpt: Massive language models can be accurately pruned in one-shot. 2023.

Gene H Golub and Charles F Van Loan. *Matrix computations*. JHU press, 2013.

Babak Hassibi and David Stork. Second order derivatives for network pruning: Optimal brain surgeon. *Advances in neural information processing systems*, 5, 1992.

Edward J Hu, Yelong Shen, Phillip Wallis, Zeyuan Allen-Zhu, Yuanzhi Li, Shean Wang, Lu Wang, and Weizhu Chen. Lora: Low-rank adaptation of large language models. *arXiv preprint arXiv:2106.09685*, 2021.

Itay Hubara, Yury Nahshan, Yair Hanani, Ron Banner, and Daniel Soudry. Accurate post training quantization with small calibration sets. In *International Conference on Machine Learning*, pp. 4466–4475. PMLR, 2021.

Alexander Immer, Tycho van der Ouderaa, Gunnar Rätsch, Vincent Fortuin, and Mark van der Wilk. Invariance learning in deep neural networks with differentiable laplace approximations. *Advances in Neural Information Processing Systems*, 35:12449–12463, 2022.

Abdoulaye Koroko, Ani Anciaux-Sedrakian, Ibtihel Ben Gharbia, Valérie Garès, Mounir Haddou, and Quang Huy Tran. Efficient approximations of the fisher matrix in neural networks using kronecker product singular value decomposition. *arXiv preprint arXiv:2201.10285*, 2022.

Frederik Kunstner, Philipp Hennig, and Lukas Balles. Limitations of the empirical fisher approximation for natural gradient descent. *Advances in neural information processing systems*, 32, 2019.

Eldar Kurtic, Daniel Campos, Tuan Nguyen, Elias Frantar, Mark Kurtz, Benjamin Fineran, Michael Goin, and Dan Alistarh. The optimal bert surgeon: Scalable and accurate second-order pruning for large language models. *arXiv preprint arXiv:2203.07259*, 2022.

Yann LeCun, John Denker, and Sara Solla. Optimal brain damage. *Advances in neural information processing systems*, 2, 1989.

Christos Louizos, Max Welling, and Diederik P Kingma. Learning sparse neural networks through l_0 regularization. *arXiv preprint arXiv:1712.01312*, 2017.

David JC MacKay. *Information theory, inference and learning algorithms*. Cambridge university press, 2003.

James Martens and Roger Grosse. Optimizing neural networks with kronecker-factored approximate curvature. In *International conference on machine learning*, pp. 2408–2417. PMLR, 2015.

Stephen Merity, Caiming Xiong, James Bradbury, and Richard Socher. Pointer sentinel mixture models. *arXiv preprint arXiv:1609.07843*, 2016.

Mingjie Sun, Zhuang Liu, Anna Bair, and J Zico Kolter. A simple and effective pruning approach for large language models. *arXiv preprint arXiv:2306.11695*, 2023.

Hugo Touvron, Louis Martin, Kevin Stone, Peter Albert, Amjad Almahairi, Yasmine Babaei, Niko-lay Bashlykov, Soumya Batra, Prajjwal Bhargava, Shruti Bhosale, et al. Llama 2: Open foundation and fine-tuned chat models. *arXiv preprint arXiv:2307.09288*, 2023.

Ashish Vaswani, Noam Shazeer, Niki Parmar, Jakob Uszkoreit, Llion Jones, Aidan N Gomez, Łukasz Kaiser, and Illia Polosukhin. Attention is all you need. *Advances in neural information processing systems*, 30, 2017.

Chaoqi Wang, Roger Grosse, Sanja Fidler, and Guodong Zhang. Eigendamage: Structured pruning in the kronecker-factored eigenbasis. In *International conference on machine learning*, pp. 6566–6575. PMLR, 2019.

Wikipedia. *Wikipedia*. PediaPress, 2004.

Thomas Wolf, Lysandre Debut, Victor Sanh, Julien Chaumond, Clement Delangue, Anthony Moi, Pierrick Cistac, Tim Rault, Rémi Louf, Morgan Funtowicz, et al. Huggingface’s transformers: State-of-the-art natural language processing. *arXiv preprint arXiv:1910.03771*, 2019.

Susan Zhang, Stephen Roller, Naman Goyal, Mikel Artetxe, Moya Chen, Shuohui Chen, Christopher Dewan, Mona Diab, Xian Li, Xi Victoria Lin, et al. Opt: Open pre-trained transformer language models. *arXiv preprint arXiv:2205.01068*, 2022.

Aojun Zhou, Yukun Ma, Junnan Zhu, Jianbo Liu, Zhijie Zhang, Kun Yuan, Wenxiu Sun, and Hongsheng Li. Learning n: m fine-grained structured sparse neural networks from scratch. *arXiv preprint arXiv:2102.04010*, 2021.

A DERIVATIONS FOR PRUNING

Given that we use a Gaussian approximation of our loss $p \approx q = \mathcal{N}$ through a quadratic approximation of our log likelihood $-\log p \approx \frac{1}{2}(\boldsymbol{\theta}^*)^T \mathbf{F} \boldsymbol{\theta}^*$, the most optimal compression becomes the solution to the following constrained optimization problem:

$$\begin{aligned} \arg \min_{\Delta \boldsymbol{\theta}^*} \frac{1}{2} \Delta(\boldsymbol{\theta}^*)^T \mathbf{F} \Delta \boldsymbol{\theta}^* \\ \text{s.t. } \mathbf{e}_k^T \Delta \boldsymbol{\theta}^* + \mathbf{e}_k^T \boldsymbol{\theta}^* = 0, \forall k \in Q \end{aligned} \quad (14)$$

where \mathcal{Q} is the set of Q indices that are pruned.

A.1 GENERAL SOLUTION

Following (Kurtic et al., 2022), we denote pruned elements as $\mathbf{E}_K = [\mathbf{e}_{q_1} \ \mathbf{e}_{q_2} \ \dots]^T \in [0, 1]^{|\mathcal{Q}| \times P}$ and use the fact that solving eq. (6) through use of Langrange multipliers gives the general closed-form solution for cost \mathcal{L} and weight update $\Delta \boldsymbol{\theta}$:

$$\mathcal{L} = \frac{1}{2} (\mathbf{E}_K \boldsymbol{\theta}^*)^T (\mathbf{E}_K \mathbf{F}^{-1} \mathbf{E}_K^T)^{-1} \mathbf{E}_K \boldsymbol{\theta}^* \quad (15)$$

$$\Delta \boldsymbol{\theta}^* = \mathbf{F}^{-1} \mathbf{E}_K^T (\mathbf{E}_K \mathbf{F}^{-1} \mathbf{E}_K^T)^{-1} \mathbf{E}_K \boldsymbol{\theta}^* \quad (16)$$

A.2 REMOVING A SINGLE ELEMENT

Optimal brain surgeon (OBS) To remove a single element with index q , we simply set $\mathbf{E}_K = \mathbf{e}_k^T$:

$$\begin{aligned} \mathcal{L} &= \frac{1}{2} (\mathbf{E}_K \boldsymbol{\theta}^*)^T (\mathbf{E}_K \mathbf{F}^{-1} \mathbf{E}_K^T)^{-1} \mathbf{E}_K \boldsymbol{\theta} & \Delta \boldsymbol{\theta} &= -\mathbf{F}^{-1} \mathbf{E}_K^T (\mathbf{E}_K \mathbf{F}^{-1} \mathbf{E}_K^T)^{-1} \mathbf{E}_K \boldsymbol{\theta} \\ &= \frac{1}{2} \boldsymbol{\theta}_k^T \frac{1}{[\mathbf{F}^{-1}]_{kk}} \boldsymbol{\theta}_k & &= -\mathbf{F}^{-1} \mathbf{e}_k (\mathbf{e}_k^T \mathbf{F}^{-1} \mathbf{e}_k)^{-1} \mathbf{e}_k^T \boldsymbol{\theta} \\ &= \frac{1}{2} \frac{(\boldsymbol{\theta}_k)^2}{[\mathbf{F}^{-1}]_{kk}} & &= -\frac{\boldsymbol{\theta}_k}{[\mathbf{F}^{-1}]_{kk}} \mathbf{F}^{-1} \mathbf{e}_k \end{aligned} \quad (17)$$

which exactly correspond to the loss and updates of *optimal brain surgeon* (Hassibi & Stork, 1992).

Optimal brain damage (OBD) We may also consider that elements are independent and the Fisher is diagonal. After noting that this implies that diagonal elements of the inverse Fisher are scalar inverses of elements in the Fisher $[\mathbf{F}^{-1}]_{kk} = \frac{1}{[\mathbf{F}]_{kk}}$, the formula's simplify to:

$$\mathcal{L} = [\mathbf{F}]_{kk} (\boldsymbol{\theta}_k)^2, \quad \Delta \boldsymbol{\theta} = -\boldsymbol{\theta}_k \mathbf{e}_k \quad (18)$$

which exactly corresponds to loss and updates of *optimal brain damage* (LeCun et al., 1989).

VECTORISED

For implementation purposes, it might be convenient to have a vectorised notation $\mathcal{L}_{\boldsymbol{\theta}} \in \mathbb{R}^{RC}$ or $\mathcal{L}_{\mathbf{W}} \in \mathbb{R}^{R \times C}$ to calculate all expected losses in parallel:

$$\begin{aligned} \text{For OBD: } \mathcal{L}_{\boldsymbol{\theta}} &= \frac{1}{2} \boldsymbol{\theta}^* \odot \boldsymbol{\theta}^* \odot \text{diag}(\mathbf{F}) & \mathcal{L}_{\mathbf{W}} &= \frac{1}{2} \mathbf{W}^* \odot \mathbf{W}^* \odot \text{mat}(\text{diag}(\mathbf{F})) \\ \text{For OBS: } \mathcal{L}_{\boldsymbol{\theta}} &= \frac{1}{2} \boldsymbol{\theta}^* \odot \boldsymbol{\theta}^* \oslash \text{diag}(\mathbf{F}^{-1}), & \mathcal{L}_{\mathbf{W}} &= \frac{1}{2} \mathbf{W}^* \odot \mathbf{W}^* \oslash \text{mat}(\text{diag}(\mathbf{F}^{-1})) \end{aligned} \quad (19)$$

A.3 REMOVING A SINGLE ROW OR COLUMN

Structured OBS If we consider the approximation $\mathbf{F} \approx \mathbf{G} \otimes \mathbf{A}$ with known inverse $(\mathbf{G} \otimes \mathbf{A})^{-1} = \mathbf{G}^{-1} \otimes \mathbf{A}^{-1}$, then to remove a row at index $r \in [0, R]$, we must take into account correlations within

elements of that row. That is, we write matrix $\mathbf{E}_K = (\mathbf{e}_r^T \otimes \mathbf{I})$ containing one-hot row-vectors for all elements in row r . Plugging into the general solution eq. (7), we find:

$$\begin{aligned}
\mathcal{L} &= \frac{1}{2} \mathbf{E}_K \boldsymbol{\theta}^T (\mathbf{E}_K \mathbf{F}^{-1} \mathbf{E}_K^T)^{-1} \mathbf{E}_K \boldsymbol{\theta}^* \\
&= \frac{1}{2} ((\mathbf{e}_r^T \otimes \mathbf{I}) \boldsymbol{\theta}^*)^T ((\mathbf{e}_r^T \otimes \mathbf{I}) (\mathbf{G} \otimes \mathbf{A})^{-1} (\mathbf{e}_r^T \otimes \mathbf{I})^T)^{-1} (\mathbf{e}_r^T \otimes \mathbf{I}) \boldsymbol{\theta}^* \\
&= \frac{1}{2} \boldsymbol{\theta}_r^T (\mathbf{e}_r^T \mathbf{G}^{-1} \mathbf{e}_r \otimes \mathbf{I} \mathbf{A}^{-1} \mathbf{I})^{-1} \boldsymbol{\theta}_r \\
&= \frac{1}{2} \boldsymbol{\theta}^T (\mathbf{e}_r^T \otimes \mathbf{I}) ([\mathbf{G}^{-1}]_{rr}] \otimes \mathbf{A}^{-1})^{-1} (\mathbf{e}_r \otimes \mathbf{I}) \boldsymbol{\theta}_r \\
&= \frac{1}{2} \frac{\boldsymbol{\theta}_r^T \mathbf{A} \boldsymbol{\theta}_r}{[\mathbf{G}^{-1}]_{rr}}
\end{aligned} \tag{20}$$

where we write $\boldsymbol{\theta}_r = \mathbf{e}_r^T \mathbf{W}^* \in \mathbb{R}^C$ for the r 'th row-vector in \mathbf{W} . Similarly, we obtain the associated weight update:

$$\begin{aligned}
\Delta \boldsymbol{\theta} &= -\mathbf{F}^{-1} \mathbf{E}_K^T (\mathbf{E}_K \mathbf{F}^{-1} \mathbf{E}_K^T)^{-1} \mathbf{E}_K \boldsymbol{\theta}^* \\
&= -(\mathbf{G} \otimes \mathbf{A})^{-1} (\mathbf{e}_r^T \otimes \mathbf{I})^T ((\mathbf{e}_r^T \otimes \mathbf{I}) (\mathbf{G} \otimes \mathbf{A})^{-1} (\mathbf{e}_r^T \otimes \mathbf{I})^T)^{-1} (\mathbf{e}_r^T \otimes \mathbf{I}) \boldsymbol{\theta}^* \\
&= -(\mathbf{G}^{-1} \otimes \mathbf{A}^{-1}) (\mathbf{e}_r \otimes \mathbf{I}) (\mathbf{e}_r^T \mathbf{G}^{-1} \mathbf{e}_r \otimes \mathbf{A}^{-1})^{-1} \boldsymbol{\theta}_r \\
&= -\frac{1}{[\mathbf{G}^{-1}]_{rr}} (\mathbf{G}^{-1} \mathbf{e}_r \otimes \mathbf{A}^{-1} \mathbf{I} \mathbf{A}^{-1} \mathbf{I}) \boldsymbol{\theta}_r \\
&= -\frac{\mathbf{G}^{-1} \mathbf{e}_r \otimes \boldsymbol{\theta}_r}{[\mathbf{G}^{-1}]_{rr}}
\end{aligned} \tag{21}$$

arriving at a similar structured pruning update as derived in (Wang et al., 2019) for convolutional filters. We can equivalently derive expected loss and update for columns, by considering $\mathbf{E}_K = (\mathbf{I} \otimes \mathbf{e}_c^T)$. If we do so, we find the structured updates for a row r or column c :

$$\begin{aligned}
\text{Remove row } r: \quad \mathcal{L} &= \frac{1}{2} \frac{\boldsymbol{\theta}_r^T \mathbf{A} \boldsymbol{\theta}_r}{[\mathbf{G}^{-1}]_{rr}} \quad \Delta \boldsymbol{\theta} = -\frac{\mathbf{G}^{-1} \mathbf{e}_r \otimes \boldsymbol{\theta}_r}{[\mathbf{G}^{-1}]_{rr}} \\
\text{Remove column } c: \quad \mathcal{L} &= \frac{1}{2} \frac{\boldsymbol{\theta}_c^T \mathbf{G} \boldsymbol{\theta}_c}{[\mathbf{A}^{-1}]_{cc}} \quad \Delta \boldsymbol{\theta} = -\frac{\boldsymbol{\theta}_c \otimes \mathbf{A}^{-1} \mathbf{e}_c}{[\mathbf{A}^{-1}]_{cc}}
\end{aligned} \tag{22}$$

Structured OBD We may also assume that, when removing a row r , the individual elements within the row are also independent which would imply $[\mathbf{A}]_{ii} = \frac{1}{[\mathbf{A}^{-1}]_{ii}}$. Similarly, $[\mathbf{G}]_{ii} = \frac{1}{[\mathbf{G}^{-1}]_{ii}}$ when removing a column c . Consequently, we can simplify to:

$$\begin{aligned}
\text{Remove row } r: \quad \mathcal{L} &= \frac{1}{2} \mathbf{G}_{rr} \boldsymbol{\theta}_r^T \mathbf{A} \boldsymbol{\theta}_r \quad \Delta \boldsymbol{\theta} = -\mathbf{e}_r \boldsymbol{\theta}_r^T \\
\text{Remove column } c: \quad \mathcal{L} &= \frac{1}{2} \mathbf{A}_{cc} \boldsymbol{\theta}_c^T \mathbf{G} \boldsymbol{\theta}_c \quad \Delta \boldsymbol{\theta} = -\boldsymbol{\theta}_c \mathbf{e}_c^T
\end{aligned} \tag{23}$$

similar form to structured OBD losses and updates as derived in (Wang et al., 2019) for convolutional filters. The derivations slightly differ in that we start from the general solution eq. (8), circumventing the need to rederive a Langrange multipliers for each possible structure.

A.4 PRUNING MULTIPLE (CORRELATED) ROWS AND COLUMNS

Let us consider the removal of R' rows $r_1, r_2, \dots, r_{R'}$ or C' columns with indices $c_1, c_2, \dots, c_{C'}$, with $1 < R' < R$ and $1 < C' < C$. We denote matrices containing one-hot vectors selecting all rows and columns to be removed respectively as:

$$\mathbf{E}_{R'} = [\mathbf{e}_1 \ \mathbf{e}_2 \ \dots \ \mathbf{e}_{R'}]^T \in \mathbb{R}^{R' \times R} \quad \mathbf{E}_{C'} = [\mathbf{e}_1 \ \mathbf{e}_2 \ \dots \ \mathbf{e}_{C'}]^T \in \mathbb{R}^{C' \times C} \tag{24}$$

Then, the matrix \mathbf{E}_K containing one-hot row vectors selecting all elements to be removed can be written as:

$$\begin{aligned}
\text{Multiple rows:} \quad \mathbf{E}_K &= (\mathbf{E}_{R'} \otimes \mathbf{I}_C) \in \mathbb{R}^{Q \times RC}, \text{ (with } Q = R' C) \\
\text{Multiple columns:} \quad \mathbf{E}_K &= (\mathbf{I}_R \otimes \mathbf{E}_{C'}) \in \mathbb{R}^{Q \times RC}, \text{ (with } Q = RC')
\end{aligned} \tag{25}$$

To simultaneously remove rows and columns, we can stack the matrices with duplicate row vectors removed:

$$\text{Multiple rows and columns: } \mathbf{E}_K \begin{bmatrix} \mathbf{E}_{R'} \otimes \mathbf{I}_C \\ \mathbf{I}_R \otimes \mathbf{E}_{C'} \end{bmatrix} \in \mathbb{R}^{Q \times RC} \text{ with duplicate rows removed} \quad (26)$$

The removal of duplicate rows is required due to the few $R'C'$ overlapping elements between rows and columns, after which the total number of rows thus becomes $Q = R'C + C'R - R'C'$. We used appropriately sized identity matrices $\mathbf{I}_R \in \mathbb{R}^{R \times R}$ and $\mathbf{I}_C \in \mathbb{R}^{C \times C}$. For brevity, we write the vector or matrix of pruned weights $\bar{\theta} := \mathbf{E}_K \theta \in \mathbb{R}^Q$.

First, we derive the removal for R' rows by defining removal matrix as $\mathbf{E}_K = \mathbf{E}_{R'} \otimes \mathbf{I}$ and define $\bar{\mathbf{W}} := \mathbf{E}_{R'} \mathbf{W} \in \mathbb{R}^{R' \times C}$. The complete weight update for the removal of multiple rows becomes:

$$\begin{aligned} \Delta \theta &= -\mathbf{F}^{-1} \mathbf{E}_K^T (\mathbf{E}_K \mathbf{F}^{-1} \mathbf{E}_K^T)^{-1} \mathbf{E}_K \theta^* \\ &= -(\mathbf{G} \otimes \mathbf{A})^{-1} (\mathbf{E}_{R'} \otimes \mathbf{I})^T ((\mathbf{E}_{R'} \otimes \mathbf{I})(\mathbf{G} \otimes \mathbf{A})^{-1} (\mathbf{E}_{R'} \otimes \mathbf{I})^T)^{-1} (\mathbf{E}_{R'} \otimes \mathbf{I}) \theta^* \\ &= -(\mathbf{G}^{-1} \mathbf{E}_{R'}^T \otimes \mathbf{A}^{-1}) (\mathbf{E}_{R'} \mathbf{G}^{-1} \mathbf{E}_{R'}^T \otimes \mathbf{A}^{-1})^{-1} \bar{\theta}^* \\ &= -(\mathbf{G}^{-1} \mathbf{E}_{R'}^T \otimes \mathbf{A}^{-1}) ((\mathbf{E}_{R'} \mathbf{G}^{-1} \mathbf{E}_{R'}^T)^{-1} \otimes \mathbf{A}) \bar{\theta}^* \\ \Delta \mathbf{W} &= -\mathbf{G}^{-1} \mathbf{E}_{R'}^T ((\mathbf{E}_{R'} \mathbf{G}^{-1} \mathbf{E}_{R'}^T)^{-1} \bar{\mathbf{W}} \mathbf{A}) \mathbf{A}^{-1} \\ &= -\mathbf{G}^{-1} \mathbf{E}_{R'}^T (\mathbf{E}_{R'} \mathbf{G}^{-1} \mathbf{E}_{R'}^T)^{-1} \bar{\mathbf{W}} \end{aligned} \quad (27)$$

Similarly, we derive the removal of C' columns by defining removal matrix as $\mathbf{E}_K = \mathbf{I} \otimes \mathbf{E}_{C'}$ and define $\bar{\mathbf{W}} := \mathbf{E}_{C'} \mathbf{W} \in \mathbb{R}^{R \times C'}$. The complete weight update for multiple column removal becomes:

$$\begin{aligned} \Delta \theta &= -\mathbf{F}^{-1} \mathbf{E}_K^T (\mathbf{E}_K \mathbf{F}^{-1} \mathbf{E}_K^T)^{-1} \mathbf{E}_K \theta^* \\ &= -(\mathbf{G} \otimes \mathbf{A})^{-1} (\mathbf{I} \otimes \mathbf{E}_{C'})^T ((\mathbf{I} \otimes \mathbf{E}_{C'})(\mathbf{G} \otimes \mathbf{A})^{-1} (\mathbf{I} \otimes \mathbf{E}_{C'})^T)^{-1} (\mathbf{I} \otimes \mathbf{E}_{C'}) \theta^* \\ &= -(\mathbf{G} \otimes \mathbf{A})^{-1} (\mathbf{I} \otimes \mathbf{E}_{C'})^T ((\mathbf{I} \otimes \mathbf{E}_{C'})(\mathbf{G} \otimes \mathbf{A})^{-1} (\mathbf{I} \otimes \mathbf{E}_{C'})^T)^{-1} (\mathbf{I} \otimes \mathbf{E}_{C'}) \theta^* \\ &= -(\mathbf{G}^{-1} \otimes \mathbf{A}^{-1} \mathbf{E}_{C'}^T) (\mathbf{G} \otimes \mathbf{E}_{C'} \mathbf{A}^{-1} \mathbf{E}_{C'}^T)^{-1} \bar{\theta} \\ \Delta \mathbf{W} &= -\mathbf{G}^{-1} \bar{\mathbf{W}} (\mathbf{E}_{C'} \mathbf{A}^{-1} \mathbf{E}_{C'}^T)^{-1} (\mathbf{A}^{-1} \mathbf{E}_{C'}^T) \\ &= -\bar{\mathbf{W}} (\mathbf{E}_{C'} \mathbf{A}^{-1} \mathbf{E}_{C'}^T)^{-1} (\mathbf{A}^{-1} \mathbf{E}_{C'}^T) \end{aligned} \quad (28)$$

B EXPERIMENTAL DETAILS.

Code will be made available upon acceptance.

B.1 MODELS

OPT models From the OPT model family ((Zhang et al., 2022)), we consider models with the following number of parameters: 125 million (125m), 1.3 billion (1.3b), 2.7 billion (2.7b), 6.7 billion (6.7b) models. We omit 350 million model due to different layer norm. We obtain the standard pre-trained checkpoints using Huggingface (Wolf et al., 2019) and use this as a baseline and initialisation for compression.

Llama-v2 models From the Llama-v2 model family ((Touvron et al., 2023)), we consider a model with 7 billion (7b) parameters and a model with 13 billion (13b) parameters. We obtain the standard pre-trained checkpoints using Huggingface (Wolf et al., 2019) and use this as a baseline and initialisation for compression.

B.2 DATASETS

English / Wikitext-2 The majority of the results are obtained on the Wikitext-2 dataset containing parsed subsets of the English Wikipedia (Merity et al., 2016; Wikipedia, 2004), using the default training and test sets. For fitting, we use 128 batches of 2048 characters and for testing we use the standard test set containing 4358 characters.

French / Wikipedia For French data experiments, we use a subset of French wikipedia (Wikipedia, 2004). For fitting, we use 128 batches of 2048 characters and for testing we use a randomly selected test set containing 1067888 characters.

German / Wikipedia For the Italian data experiments, we use a subset of the German wikipedia (Wikipedia, 2004). For fitting, we use 128 batches of 2048 characters and for testing we use a randomly selected test set containing 1112372 characters.

Italian / Wikipedia For the Italian data experiments, we use a subset of the Italian wikipedia (Wikipedia, 2004). For fitting, we use 128 batches of 2048 characters and for testing we use a randomly selected test set containing 633177 characters.

B.3 MASK EQUIVALENCE

When comparing the equivalence of obtained pruning masks between two models θ_A and θ_B obtained by two compression methods A and B . We always consider the case of 50% pruning, and define the mask equivalence as the fraction of same weights that are set two zero in both models:

$$\text{mask equivalence} = \sum_{i=1}^P \frac{\mathbf{1}([\theta_A]_i = 0 \text{ and } [\theta_B]_i = 0)}{P}. \quad (29)$$

where $\mathbf{1}$ denotes an indicator function that returns 1 if both weights $[\theta_A]_i$ and $[\theta_B]_i$ are zero, and returns 0 otherwise.

B.4 SPARSEGPT AND EVALUATION OF BASELINES

For the SparseGPT baseline, we used the official code SparseGPT code repository (Frantar & Alis tarh, 2023) which allows for training and evaluation on wikitext-2. The obtained results may differ from those reported in the original paper as the C4 dataset was used there.

In this work, models were trained with the same 128 batches of the wikitext-2 training set as available in the SparseGPT codebase and are evaluated on the wikitext-2 test set using the exact same evaluation procedure.

C TECHNICAL DETAILS

C.1 PSEUDOCODES

Algorithm 2 LLM Surgeon (*structured*)

Input: target size α
Input: initial weights θ^0
For shot t in $[1, 2, \dots, T]$
 Compute: approximate curvature $\mathbf{G}_1, \mathbf{A}_1$ from data (optionally also $\mathbf{G}_2, \mathbf{A}_2$) \triangleright section 3.1
 Compute: costs per row/column $\mathcal{L}_r, \mathcal{L}_c$ from $\mathbf{G}_1, \mathbf{A}_1, (\mathbf{G}_2, \mathbf{A}_2)$ \triangleright section 3.2
 Compute: threshold τ using \mathcal{L}_r and \mathcal{L}_c given target size α \triangleright section 3.3
 Select: rows and columns to remove $\mathbf{E}_R, \mathbf{E}_C$ based on τ \triangleright section 3.3
 Compute: weight update $\Delta\theta^{t-1}$ based on $\mathbf{E}_R, \mathbf{E}_C$ and $\mathbf{G}_1, \mathbf{A}_1, (\mathbf{G}_2, \mathbf{A}_2)$ \triangleright section 3.4
 Update: remaining weights $\theta^t \leftarrow \theta^{t-1} + \Delta\theta^{t-1}$ \triangleright section 3.5
 Optionally: $\theta^t \leftarrow$ low-rank update(θ^t)
Output: compressed weights $\hat{\theta} = \theta^T$

Algorithm 3 LLM Surgeon (*semi-structured / unstructured*)

Input: target size α
Input: initial weights θ^0
For shot t in $[1, 2, \dots, T]$
 Compute: approximate curvature $\mathbf{G}_1, \mathbf{A}_1$ from data (optionally also $\mathbf{G}_2, \mathbf{A}_2$) \triangleright section 3.1
 Compute: costs per element \mathcal{L}_k from $\mathbf{G}_1, \mathbf{A}_1, (\mathbf{G}_2, \mathbf{A}_2)$ \triangleright section 3.2
 Compute: threshold τ from \mathcal{L}_k and target size α_t (unstructured/semistructured) \triangleright section 3.3
 Select: elements to remove \mathbf{E}_K based on τ (unstructured/semistructured) \triangleright section 3.3
 Compute: weight update $\Delta\theta^{t-1}$ based on \mathbf{E}_K and $\mathbf{G}_1, \mathbf{A}_1, (\mathbf{G}_2, \mathbf{A}_2)$ \triangleright section 3.4
 Update: remaining weights $\theta^t \leftarrow \theta^{t-1} + \Delta\theta^{t-1}$ \triangleright section 3.5
 Optionally: $\theta^t \leftarrow$ low-rank update(θ^t)
Output: compressed weights $\hat{\theta} = \theta^T$

C.2 DAMPENING

In practice, we dampen the \mathbf{G} and \mathbf{A} matrices by adding a diagonal term $\mathbf{G} + \lambda_G \mathbf{I}$ and $\mathbf{A} + \lambda_A \mathbf{I}$. In our experiments, we found that values in the range $[0.01, 0.1]$ multiplied by mean diagonal terms generally works well. We follow (Frantar & Alistarh, 2023) and always use $\lambda_A=0.01\text{diag}(\mathbf{A})$ to be consistent with prior work and allow for a fair comparison with baselines. Further, we use $\lambda_G=0.1\text{diag}(\mathbf{G})$ for structured experiments and $\lambda_G=0.01\text{diag}(\mathbf{G})$ in semi-structured and unstructured experiments.

D DOWNSTREAM TASK PERFORMANCE

We also evaluate our method on downstream tasks as perplexity metrics do not necessarily correlate with downstream performance. Further, we also repeat this experiment using the C4 dataset as reference data for compression, as this is used in prior work (Frantar & Alistarh, 2023) and as this can be regarded a more general reference dataset. In tables 5 and 6 we report 0-shot test performance of structured pruning for LLM surgeon and K-OBD baseline.

Table 5: Downstream task performance using Wikitext-2 for pruning.

Structured pruning (with wikitext-2)	Model size	wikitext word ppl	boolq	pqa	hellaswag	winogrande	arc-easy	arc-challenge	openbookq	copa	lambda.openai	wsc273	AVERAGE wikitext2
Dense baseline	100%	9.24	77.74	79.11	75.99	69.14	74.58	46.35	44.20	86.00	73.92	85.71	71.26
LLM Surgeon (ours)	90%	9.63	76.21	78.56	75.39	67.64	74.12	46.50	43.60	85.00	72.64	84.98	70.46
	80%	12.16	72.97	77.09	71.30	66.30	71.36	41.89	41.80	87.00	56.43	80.22	66.66
	70%	16.91	61.25	72.56	60.72	61.09	63.09	36.69	38.80	81.00	28.33	76.56	58.11
	60%	25.15	44.98	69.26	48.04	54.38	52.31	30.29	36.80	78.00	11.72	68.50	49.43
	50%	43.68	39.60	64.36	40.29	52.57	44.91	26.28	30.80	74.00	6.52	61.54	44.09
K-OBD	90%	9.89	76.67	78.02	74.80	68.11	75.17	46.33	44.60	86.00	72.71	82.78	70.52
	80%	17.62	74.34	75.24	67.85	64.64	63.80	40.27	41.60	83.00	30.23	82.42	62.34
	70%	32.72	65.29	71.82	53.07	56.83	51.05	33.11	37.80	79.00	12.21	70.70	53.09
	60%	68.63	60.80	65.67	43.99	53.20	41.79	28.50	34.00	75.00	7.04	60.44	47.04
	50%	136.33	61.56	60.66	36.84	53.04	36.11	26.71	33.00	72.00	4.70	61.17	44.58

Table 6: Downstream task performance using C4 for pruning.

Structured pruning (with C4)	Model size	wikitext word ppl	boolq	pqa	hellaswag	winogrande	arc-easy	arc.challenge	openbookq	copa	lambda.openai	wsc273	AVERAGE wikitext2
Dense baseline	100%	9.24	77.74	79.11	75.99	69.14	74.58	46.25	44.20	86.00	73.92	85.71	71.26
LLM Surgeon (ours)	90%	9.90	77.03	78.45	74.95	68.27	73.19	45.99	44.60	84.00	72.81	82.78	70.21
	80%	14.42	75.60	76.82	69.71	63.85	70.29	41.30	42.80	87.00	45.53	82.42	65.53
	70%	25.16	66.39	72.85	58.11	56.83	62.16	34.47	38.40	80.00	22.69	69.96	56.19
	60%	45.35	62.48	68.93	48.10	55.64	51.56	27.99	35.20	70.00	12.56	61.54	49.40
	50%	77.30	62.60	65.02	41.70	54.22	42.55	24.23	31.20	71.00	7.26	60.44	46.02
K-OBD	90%	10.59	75.47	78.18	73.61	66.46	72.52	44.37	43.60	87.00	71.22	82.42	69.48
	80%	20.12	73.36	75.14	66.11	62.43	62.84	38.23	41.00	86.00	21.50	78.39	60.50
	70%	36.92	63.30	68.44	52.31	55.64	46.72	31.31	34.60	77.00	5.69	68.86	50.39
	60%	112.85	62.23	64.47	46.36	52.17	40.53	29.52	32.40	72.00	2.91	63.00	46.56
	50%	272.16	62.42	61.70	38.47	50.43	33.29	26.96	31.80	65.00	0.91	59.34	43.03

We find that our method not only performs well in terms of test perplexity but also correlates well with downstream performance, outperforming the baselines on these downstream tasks.

E ADDITIONAL EXPERIMENTS ON LLAMA-V2 13B.

To assess performance on larger 13B parameter models, we also report structured compression on the Llama-v2 13B model and evaluate downstream task performance. Test perplexities (lower is better) can be found in table 7 below:

Table 7: Pruning Llama-v2 13B model.

Baseline	Pruned model sizes					
	90%	80%	70%	60%	50%	
K-OBD	4.547	4.908	6.294	10.08	13.06	16.06
LLM Surgeon	4.547	4.692	5.286	6.207	7.245	9.428

as well as evaluated results on downstream benchmarks (higher is better) in table 8 below.

Table 8: Downstream task performance after pruning large Llama-v2 13B model.

Llama-v2 13B	Model size	wikitext word ppl	boolq	pqa	hellaswag	winogrande	arc-easy	arc.challenge	openbookq	copa	lambda.openai	wsc273	AVERAGE wikitext2
Dense baseline	100%	8.23	80.52%	80.52%	79.38%	72.14%	77.53%	49.23%	45.20%	90.00%	76.77%	89.38%	74.07%
LLM Surgeon (ours)	90%	8.57	81.07%	79.87%	79.24%	72.38%	76.30%	49.91%	47.20%	92.00%	75.47%	89.38%	74.28%
	80%	10.08	80.86%	79.60%	77.09%	70.56%	75.93%	46.76%	46.80%	90.00%	67.79%	86.45%	72.12%
	70%	12.74	74.50%	76.50%	71.52%	68.67%	69.74%	40.27%	45.00%	91.00%	54.40%	83.52%	67.51%
	60%	16.00	64.62%	73.01%	65.04%	65.75%	63.80%	37.12%	39.60%	90.00%	44.50%	81.32%	62.48%
	50%	23.75	65.66%	68.77%	56.19%	63.22%	56.19%	31.83%	36.60%	85.00%	35.16%	77.29%	57.59%
K-OBD	90%	8.79	81.31%	79.76%	79.12%	72.22%	76.94%	47.95%	47.80%	91.00%	75.26%	88.64%	74.00%
	80%	11.79	80.80%	79.16%	76.80%	70.56%	73.74%	46.93%	48.60%	88.00%	58.54%	87.55%	71.11%
	70%	20.00	66.76%	74.43%	64.18%	64.96%	56.23%	38.01%	39.00%	88.00%	38.54%	79.49%	60.76%
	60%	27.74	55.66%	70.24%	55.52%	60.46%	49.62%	32.88%	33.00%	80.00%	30.06%	73.63%	54.37%
	50%	37.38	59.79%	66.54%	48.39%	57.46%	46.59%	30.72%	34.00%	77.00%	24.61%	69.96%	51.50%

We find that LLM Surgeon also outperforms baselines on existing Llama-v2 13B models. We stress that these results are obtained on structured pruning of rows and columns, which are regarded the hardest and most constrained pruning structure. Yet, we can compress Llama 13B by 20% with less than 2% drop in downstream task performance. It also significantly outperforms the baseline for all compression rates, both in terms of test perplexity and downstream task performance.

F ABLATIONS

F.1 SHOTS

Table 9: Ablation of shot counts T for structured LLM Surgeon compressing OPT-1.3b model.

Target size	Shots T	wikitext-2 PPL	Shots T	wikitext-2 PPL	Shots T	wikitext-2 PPL
90%	6	14.70	8	14.70	10	14.72
80%	12	15.14	16	15.12	20	15.08
70%	18	16.21	24	16.24	30	16.23
60%	24	18.53	32	18.45	40	18.49
50%	30	23.32	40	22.95	50	22.68

F.2 TASK-SPECIFIC COMPRESSION

LLM Surgeon uses data to find a compressed model that has the least negative impact on final test performance. In this section, we explore the extent to which the method can use data to compress specifically to the task at hand. We do so by comparing test performance and equivalences between resulting pruning masks for different language modeling languages: English (EN/wikitext-2), French (FR) and Italian (IT) and the German (DE). We consider 50% unstructured compression using LLM Surgeon with correlated weight updates. For each compressed model, we compare performance on all languages and compare the equivalences between resulting pruning masks (details in appendix B.3), and report results in table 10. Like other methods that use data for compression (Hassibi & Stork, 1992; Frantar & Alistarh, 2023; Wang et al., 2019), we expect to see some correlation between the data used for training and data with good test performance, which is reflected in both test performance and masks. It is important to note that the final performance after compression will depend on the quality of the used dataset for compression. Further, the experiment demonstrates that the method can be used for task-specific compression tailored towards the data used for compression and generalises to high test performance on the associated test data.

Table 10: Cross-task performance and mask equivalences of 50% compressed OPT-125m model using structured LLM Surgeon on language subsets.

target	evaluation dataset				mask equivalence (%)			
	EN	FR	DE	IT	EN	FR	DE	IT
Pretrained	27.66	22.54	24.32	27.66	1.00	0.74	0.70	0.72
EN	47.46	172.9	181.1	169.1	0.74	1.00	0.87	0.90
FR	113.4	28.44	35.02	34.90	0.70	0.87	1.00	0.87
DE	142.1	35.15	27.49	38.49	0.72	0.90	0.87	1.00
IT	123.7	31.85	33.78	30.58	0.72	0.90	0.87	1.00

G ON FAIR COMPARISON

All results in this work (including the SparseGPT) were trained on Wikitext-2 for fair comparison. To do so, we used the same dataloader and evaluation script as the official SparseGPT repo and reran all SparseGPT results to be trained on Wikitext-2. In some cases, this resulted in better scores for the SparseGPT baseline compared to the C4-trained results reported in the original SparseGPT paper. Yet, we find that our method using improved curvature estimates still outperformed the baselines in terms of final test performance.

H COMPUTATIONAL PERFORMANCE

We report computational cost in terms of pruning time in table 11 and GPU memory in table 12.

Table 11: Time performance.

Runtime	Network	Time	Test performance				
			PPL 90%	PPL 80%	PPL 70%	PPL 60%	PPL 50%
Unstructured baseline (SparseGPT)	Llama-v2 7B	<5m	5.49	5.58	5.71	5.94	6.51
Unstructured LLM Surgeon (ours)	Llama-v2 7B	2d8h16m	5.13	5.20	5.36	5.66	6.08
Structured baseline (K-OBD)	Llama-v2 7B	16h58m	5.48	9.14	15.43	28.03	46.64
Structured LLM Surgeon (ours)	Llama-v2 7B	17h08m	5.25	6.18	7.83	10.39	15.38
Structured baseline (K-OBD)	Llama-v2 13B	1d6h5m	4.908	6.294	10.08	13.06	16.06
Structured LLM Surgeon (ours)	Llama-v2 13B	1d9h26m	4.692	5.286	6.207	7.245	9.428

Our method is most efficient for structured pruning, but it must be noted that engineering efforts may further improve speed for unstructured pruning. The focus of the paper is structured pruning, on which we achieve state-of-the-art compression rates. Importantly, compression of LLMs only needs to happen once after which a pruned model can be deployed infinitely many times without further cost. This motivates our method which takes longer to run but reaches better final test performance.

Table 12: Memory performance.

Network	SparseGPT (baseline)	Unstructured LLM-Surgeon (ours)
Llama-7B	<5m / 1 GPU (32GB)	2d8h16m / 4xH100 80 GB
	K-OBD (baseline)	Structured LLM-Surgeon (ours)
Llama-7B	16h58m / 4xH100 80 GB	17h08m / 4xH100 80 GB
Llama-13B	1d6h5m / 8xH100 80 GB	1d9h26m / 8xH100 80 GB

We argue that differences in the performance and the runtime of pruning methods can largely be attributed to underlying assumptions on correlations between weights. Notably, algorithms that consider few correlations, sometimes to the extent of completely disregarding all gradient information, can result in very fast pruning algorithms for unstructured and semi-structured pruning but are often not flexible enough to perform structured pruning of rows and columns. Examples of such lightweight algorithms for LLMs are (Sun et al., 2023) and SparseGPT (Frantar & Alistarh, 2023), as can also be observed from table 11. Our approach makes less strong assumptions on the curvature of the loss and as a result outperforms all baselines on all unstructured, semi-structured and structured pruning. Further, the improved curvature is also eligible for dynamic allocation of weight removal and improved correlated weight updates. In practice, we always recommend using our method for structured pruning. For unstructured and semi-structured pruning, we note an important trade-off between the desired final test accuracy and the available computational budget. Here, our proposed method can achieve the highest final model performance but requires more computational resources and takes longer to run. It should be noted that pruning only needs to happen once after which a model can be deployed infinitely many times this time, which dependent on the available computational resources can also legitimise spending additional pruning time even if this is much higher compared to other algorithms in relative terms. In absolute terms, the use of multiple large GPUs is common practice in the field of large language models and many more GPUs are typically used to train and deploy large language models. Moreover, the curvature approximation is naively amenable to data parallelism in case further speed-ups or larger models are required. We hope this provides context and emphasises the trade-off between performance and compute in practice.

I EXTENDING CURVATURE ESTIMATES

Instead of using a single Kronecker product, we might consider improving the approximation through a sum of multiple Kronecker factors:

$$\mathbf{F} \approx \tilde{\mathbf{F}} = \mathbf{G}_1 \otimes \mathbf{A}_1 + \mathbf{G}_2 \otimes \mathbf{A}_2 \quad (30)$$

This last appendix deals with the question how one may computationally find such approximations and how to utilise them in the neural network pruning framework.

I.1 NEAREST KRONECKER PRODUCT OR SUM OF KRONECKER PRODUCTS

Instead of assuming independence of activations and derivatives as in section 3.1, following the classic KFAC of (Martens & Grosse, 2015), we might want to find the *nearest Kronecker product* approximation $\mathbf{F} \approx \tilde{\mathbf{G}} \otimes \tilde{\mathbf{A}}$ that is closest to the Fisher in terms of the Frobenius norm:

$$\tilde{\mathbf{G}}_l, \tilde{\mathbf{A}}_l = \arg \min_{\mathbf{G}_l, \mathbf{A}_l} \|\mathbf{F}_l - \mathbf{G}_l \otimes \mathbf{A}_l\|_F \quad (31)$$

Finding the nearest sum of Kronecker factors can be rephrased as a classic eigenvalue problem of finding the nearest rank-1 matrix. Golub & Van Loan (2013).

$$\|\mathbf{F} - \tilde{\mathbf{G}} \otimes \tilde{\mathbf{A}}\|_F \equiv \|\mathcal{R}(\mathbf{F}) - \text{vec}(\tilde{\mathbf{G}})\text{vec}(\tilde{\mathbf{A}})^T\|_F \quad (32)$$

Power method and deflation After considering the reshaping, we can use power iterations to solve for and find the nearest Kronecker factors $\mathbf{G}_1, \mathbf{A}_1 = \text{solve}(\mathbf{F})$.

Find with power iterations:

$$\tilde{\mathbf{G}}_1, \tilde{\mathbf{A}}_1 = \text{solve}(\mathbf{F}) = \arg \min_{\mathbf{G}, \mathbf{A}} \|\mathbf{F} - \mathbf{G} \otimes \mathbf{A}\|_F \quad \tilde{\mathbf{G}}_r, \tilde{\mathbf{A}}_r = \text{solve}(\mathbf{F} - \sum_{r'=1}^{r-1} (\tilde{\mathbf{G}}_{r'} \otimes \tilde{\mathbf{A}}_{r'}))$$

Deflation:

A more extensive description of the power method `solve`(\cdot) can be found in algorithm 4. At the start of the algorithm, we initialise power iterations as vector with one's $\mathbf{1} = [1 \ 1 \ \dots \ 1]$. After each shot we can initialise the vector as the final estimate found during the previous shot.

Algorithm 4 Kronecker power method. Finds $\tilde{\mathbf{G}}, \tilde{\mathbf{A}}$ nearest Kronecker product $\|\mathbf{F} - \tilde{\mathbf{G}} \otimes \tilde{\mathbf{A}}\|_F$.

Input: Initialise $\tilde{\mathbf{g}}^0 = \mathbf{1}, \tilde{\mathbf{a}}^0 = \mathbf{1}$ (or using estimates of previous shot).

Input: Set iterations I (or $I=1$ if using estimates from previous shot)

Output: $\tilde{\mathbf{G}}, \tilde{\mathbf{A}}$

for iteration i in $[1, 2, \dots, I]$ **do**

Compute: $\tilde{\mathbf{g}}^i = \frac{\mathcal{R}(\tilde{\mathbf{F}})\tilde{\mathbf{a}}^{i-1}}{\|\mathcal{R}(\tilde{\mathbf{F}})\tilde{\mathbf{a}}^{i-1}\|_2}$, with $\mathcal{R}(\tilde{\mathbf{F}})\tilde{\mathbf{a}}^{i-1} = \frac{1}{N} \sum_{n=1}^N \mathbf{a}_n^T \tilde{\mathbf{A}}^{i-1} \mathbf{a}_n \text{vec}(\mathbf{g}_n \mathbf{g}_n^T)$

Compute: $\tilde{\mathbf{a}}^i = \frac{\mathcal{R}(\tilde{\mathbf{F}})^T \tilde{\mathbf{g}}^i}{\|\mathcal{R}(\tilde{\mathbf{F}})^T \tilde{\mathbf{g}}^i\|_2}$, with $\mathcal{R}(\tilde{\mathbf{F}})^T \tilde{\mathbf{g}}^i = \frac{1}{N} \sum_{n=1}^N \mathbf{g}_n^T \tilde{\mathbf{G}}^i \mathbf{g}_n \text{vec}(\mathbf{a}_n \mathbf{a}_n^T)$

Compute: $\sigma^i = \|\tilde{\mathbf{a}}^i\|_2$

end for

Return: $\tilde{\mathbf{G}} = \sqrt{\sigma^i} \text{mat}(\tilde{\mathbf{g}}), \tilde{\mathbf{A}} = \sqrt{\sigma^i} \text{mat}(\tilde{\mathbf{a}})$.

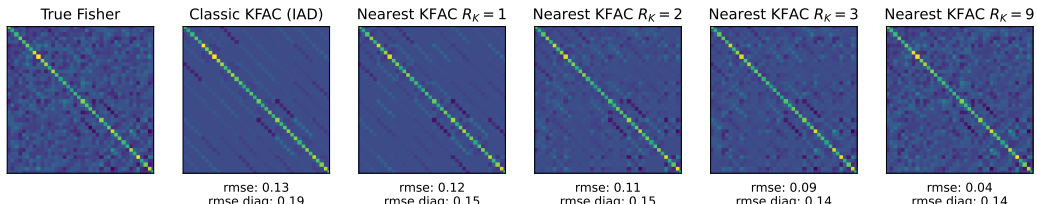


Figure 5: Example illustration of nearest Kronecker factor approximations $\tilde{\mathbf{F}} \approx \sum_{r=1}^{R_K} \mathbf{G}_r \otimes \mathbf{A}_r$, compared to classical KFAC with the IAD assumption. Larger R_K yields better approximations to the true Fisher \mathbf{F} for larger R_K , as measured by the root mean squared error (rmse).

I.2 EXTENDED CURVATURE APPROXIMATIONS

For classic KFAC with IAD or $R_K=1$ nearest Kronecker approximations of the form $\tilde{\mathbf{F}} = \mathbf{G} \otimes \mathbf{A}$, the inverse simply becomes $(\mathbf{G} \otimes \mathbf{A})^{-1} = \mathbf{G}^{-1} \otimes \mathbf{A}^{-1}$. Unfortunately, we can not use this famous inverse identity for sum of Kronecker factors, which is why we fall back on eigendecompositions $\mathbf{G} = \mathbf{E}_1 \mathbf{S}_1 \mathbf{E}_1^T$ and $\mathbf{A} = \mathbf{E}_2 \mathbf{S}_2 \mathbf{E}_2^T$, allowing us to decompose the Fisher into:

$$\tilde{\mathbf{F}} = \mathbf{K}_1 \mathbf{S}_1 \mathbf{K}_1^T \otimes \mathbf{K}_2 \mathbf{S}_2 \mathbf{K}_2^T = (\mathbf{K}_1 \otimes \mathbf{K}_2) (\mathbf{I} \otimes \mathbf{I} + \mathbf{S}_1 \otimes \mathbf{S}_2) (\mathbf{K}_1^T \otimes \mathbf{K}_2^T) \quad (33)$$

where specific \mathbf{K}_1 and \mathbf{K}_2 can be found in App. B of Martens & Grosse (2015), which we closely followed in our derivations. Because \mathbf{K}_1 and \mathbf{K}_2 are orthogonal and \mathbf{S}_1 and \mathbf{S}_2 diagonal, the inverse Fisher becomes:

$$\tilde{\mathbf{F}}^{-1} = (\mathbf{K}_1 \otimes \mathbf{K}_2) (\mathbf{I} \otimes \mathbf{I} + \mathbf{S}_1 \otimes \mathbf{S}_2)^{-1} (\mathbf{K}_1^T \otimes \mathbf{K}_2^T) \quad (34)$$

In the context of neural network training, the problem gets slightly harder since we want to incrementally construct estimates $\tilde{\mathbf{G}}_i$ and $\tilde{\mathbf{A}}_i$ from individual samples $\mathbf{a}_{l,n}, \mathbf{g}_{l,n}$ that make up \mathbf{F} , without having to simultaneously store more than a single or batch of input activations $\mathbf{a}_{l,n}$ or output gradients $\mathbf{g}_{l,n}$ in memory. Although this *online Kronecker-product principal component analysis* problem largely remains an open research problem, we our approach closely follows the recent work by (Koroko et al., 2022) that uses similar approximations in the context of optimisation. A sum of multiple $R_K > 1$ Kronecker factors will yield closer approximations, but also linearly increase memory requirements with higher R_K and makes inverting \mathbf{F}^{-1} considerably more difficult.

Formulas to compute cost and weight updates. For sum of Kronecker factors, we find that the constrained optimization solution of for costs $\Delta \mathcal{L}$ eq. (7) and weight updates $\Delta \theta$ eq. (8) become the following inner-product and matrix-vector product:

$$\mathcal{L}_k = \frac{1}{2} \langle \overline{\theta^*}, \mathbf{U} \overline{\theta^*} \rangle = (\overline{\theta^*})^T \mathbf{U} (\overline{\theta^*}) \in \mathbb{R} \quad (35)$$

$$\Delta \theta = \tilde{\mathbf{F}}^{-1} \mathbf{E}_K^T \mathbf{u} = \mathbf{K}_1 \left(\overline{\mathbf{K}_1^T} \mathbf{U} \overline{\mathbf{K}_2} \otimes [\mathbf{1} \mathbf{1}^T + \mathbf{S}_1 \mathbf{S}_2^T] \right) \mathbf{K}_2^T \in \mathbb{R}^{RC} \quad (36)$$

with at the heart of it all a matrix $\mathbf{U} = [\mathbf{E}_K \mathbf{F}^{-1} \mathbf{E}_K^T]^{-1}$ that captures correlations between weights:

$$\mathbf{U} = \left[\mathbf{E}_K \left(\mathbf{K}_1 \otimes \mathbf{K}_2 \right) \left(\mathbf{I} \otimes \mathbf{I} + \mathbf{S}_1 \otimes \mathbf{S}_2 \right)^{-1} \left(\mathbf{K}_1^T \otimes \mathbf{K}_2^T \right) \mathbf{E}_K^T \right]^{-1} \quad (37)$$

where $(\mathbf{I} \otimes \mathbf{I} + \mathbf{S}_1 \otimes \mathbf{S}_2)$ is diagonal and the inverse can thus be computed element-wise. The remaining inverse is of size $K \times K$, for K correlated weights.

Note on sum of Kronecker factors Experimentally, we did not find a benefit in performance when using a sum of two nearest Kronecker factor approximation, or found it too slow. Therefore, we focus in the main text on LLM Surgeon with fast single Kronecker product KFAC approximation to approximate the loss landscape curvature. Nevertheless, we choose to include this appendix as we believe could prove useful in other contexts or inspire future work that aim to further improve the quality of curvature approximations.